Computational Materials Science 229 (2023) 112426

Contents lists available at ScienceDirect

Computational Materials Science

journal homepage: www.elsevier.com/locate/commatsci

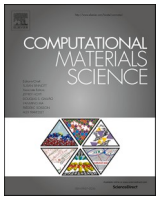

Full Length Article

The basic physical properties of Li_2MnO_3 and $LiMn_2O_4$ cathode materials

Jialiang Xu [a], Shiji Zhu [a], Zhenming Xu [b], Hong Zhu [a,*]

[a] University of Michigan–Shanghai Jiao Tong University Joint Institute, Shanghai Jiao Tong University, Shanghai 200240, China
[b] College of Materials Science and Technology, Nanjing University of Aeronautics and Astronautics, Nanjing 210016, China

ARTICLE INFO

Keywords:
First-principles calculation
Li cathode materials
Diffusion
Energy barrier
Doping

ABSTRACT

The basic physical properties of the layered lithium manganese oxide Li_2MnO_3 and the spinel lithium manganese oxide $LiMn_2O_4$ were investigated by the first-principles calculations based on density functional theory in this paper. Herein, the differences in crystal structures, electronic structures, and Li-ion transport characteristics between Li_2MnO_3 and $LiMn_2O_4$ were discussed in detail. It was found that both Li_2MnO_3 and $LiMn_2O_4$ are semiconductors, but the band gap of Li_2MnO_3 (2.1 eV) is much larger than that of $LiMn_2O_4$ (0.36 eV). The phonon dispersions show both the anti-ferromagnetic (AFM) configurations of Li_2MnO_3 and $LiMn_2O_4$ are dynamically stable. Moreover, the migration of Li ions in $LiMn_2O_4$ is faster than that in Li_2MnO_3. To further increase the Li diffusivity of Li_2MnO_3, the tetravalent dopants (Ir^{4+}, Os^{4+}, and Ru^{4+}) were considered to substitute the Mn site of Li_2MnO_3. Our theoretical results explain the higher stability of doped Li_2MnO_3 through enhancing the Li migrating ability.

1. Introduction

With the successful implementation of intelligent electronic devices, the rechargeable lithium-ion batteries (LIBs) have become an important energy storage technology today.[1,2] The cathode materials of LIBs with larger capacity and longer cycle life are the key factor restricting the energy density of the battery. Layered $LiCoO_2$, the earliest commercial cathode material, has a theoretical capacity of 273 mAh/g, but its actual available capacity is only about 140 mAh/g owing to the surface reaction and structural instability.[3].

Since Co has the disadvantages of high cost, toxicity, environmental unfriendliness and so on, many works have been devoted to the investigation of other lithium transition metal oxide cathode materials, LiTMO (TM = Mn, Ni and other transition metals), to satisfy the demand of high-performance batteries. There are other cathode materials appeared, such as Li_2MnO_3, $LiMn_2O_4$, and $LiFePO_4$,. The insertion electrodes of lithium-ion electrochemical cells need to have a stable structure over a wide range of Li concentrations to insert and extract as much lithium as possible during repeated charging and discharging processes to maximize battery capacity, energy, and cycle life.

Nowadays, layered Li_2MnO_3 is one of the most widely studied cathode materials due to high discharge capacity and rate performance.[4] The surface reconstruction of Li ions in Li_2MnO_3 is highly anisotropic, which is mainly along the lithium ion diffusion channel during the charging process. However, the stability of Li_2MnO_3 decreases significantly during the later charging process and its utilization efficiency is about 44%.[5] Meanwhile, the migration of Mn atoms in Li_2MnO_3 will cause its phase transition during the later charging process.[6,7] To block the phase transition, an effective method is to apply other transition metal elements to replace Mn atoms. Prior density functional theory (DFT) simulations suggested that the addition of Os, Sb, Ru, Ir, or Ta can improve the oxygen retention and the structure stability of Li_2MnO_3 and Ta-doping has been experimentally demonstrated to display higher electrochemical performance and better oxygen retention.[8] Besides, another method to improve the structure stability of electrode materials is by coating the spinel phase on the surface of Li-excess material.[9]

The spinel $LiMn_2O_4$, another cathode material, has a much lower theoretical capacity of 148 mAh/g compared with the Li_2MnO_3 of 459 mAh/g, but has a high utilization efficiency of 67%~81%.[10] In addition, the voids and defects in $LiMn_2O_4$ can enhance the transmission rate of Li ions. Compared with Li_2MnO_3, the spinel $LiMn_2O_4$ has a lower migration energy barrier for rapid lithium ion transport. In order to improve the cyclic stability and electrochemical performance, the spinel structure combined with the layered composite cathode materials have been extensively studied. For example, the cobalt-free layer-spinel composite cathode material $0.5Li_2MnO_3$-$0.25LiMn_2O_4$-$0.25LiNi_{0.5}Mn_{0.5}O_2$ was synthesized by the sol–gel method and exhibits

* Corresponding author.
E-mail address: hong.zhu@sjtu.edu.cn (H. Zhu).

https://doi.org/10.1016/j.commatsci.2023.112426
Received 18 April 2023; Received in revised form 30 June 2023; Accepted 1 August 2023
Available online 8 August 2023

the higher capacity retention rate and good cycle stability, and the coulomb efficiency reaches 98%.[11] A novel cathode material composed of Li-rich layered material and spinel $LiMn_2O_4$, exhibits excellent stability, high capacity and can also prevent phase transition of layered Li_2MnO_3, but the systematic comparison of the basic properties of the Li_2MnO_3 and $LiMn_2O_4$ is still in need.

In this work, the basic physical properties of Li_2MnO_3 and $LiMn_2O_4$ were thoroughly investigated based on the DFT and phonopy calculation. The lattice constants, electronic structures, Li ionic conductivities of the two materials were compared and evaluated in details. Li ion migration energy barrier is remarkable different between Li_2MnO_3 and $LiMn_2O_4$. Doping with Os, Ta, Ru, and Ir in Li_2MnO_3 would further enhance the mobility of Li ions, closer to the Li diffusion of the $LiMn_2O_4$.

2. Methods

The total energy of the system and the migration energy barrier of Li ions were calculated by first principles simulations based on Density Functional Theory (DFT)[11,12], which was implemented in Vienna ab initio Simulation Package (VASP)[13] with the projector augmented wave (PAW) pseudopotential method.[14,15] The generalized gradient approximation (GGA) with the Perdew-Burke-Ernzerhof (PBE)[16] version was chosen for all the calculations.[17,18] We test the U value of 3.9 eV, 4.5 eV and 5.0 eV for Mn in Li_2MnO_3 and $LiMn_2O_4$ to get band gaps similar to experimental values. The U parameters of 5.0 eV on Mn in Li_2MnO_3 and 3.9 eV on Mn in $LiMn_2O_4$ were chosen for the density of states calculation.[19–21] A plane-wave energy cutoff of 520 eV was set. The Gamma-centered 10 × 10 × 10 k-mesh was applied for integration in the Brillouin zone of Li_2MnO_3, while 8 × 8 × 8 k-point mesh was employed for $LiMn_2O_4$. Phonon density of states (DOS) were calculated with the PHONOPY code[22]. The conventional cell of Li_2MnO_3 and $LiMn_2O_4$ were fully relaxed for bulk calculations. The convergence criteria for structural optimization was 10^{-5} eV/atom for total energy and below 0.01 eV $Å^{-1}$ for interatomic forces. A supercell was used to investigate all Li-migrations which contain 16 f.u. (96 atoms) for Li_2MnO_3 and 8 f.u. (56 atoms) $LiMn_2O_4$ using the climbing image nudged elastic band (CINEB) method.[23] Ab initio molecular dynamics (AIMD) simulations were performed to evaluate charged Li diffusivity. A smaller plane-wave energy cutoff of 300 eV and 1 × 1 × 1 Γ-centered k-mesh were selected for AIMD simulations considering computational efficiency. All systems were simulated for 20,000 steps with a time step of 2 fs and a total time of 240 ps in the NVT ensemble using a Nose-Hoover thermostat. The energy barrier of Li_2MnO_3 after doping with transition metals was acquired with softBV software tool using the bond valence pathway analyzer (BVPA).[24] After doping, there are many different Li migration channels. BVPA is more suitable for considering all unique diffusion paths than CINEB method.

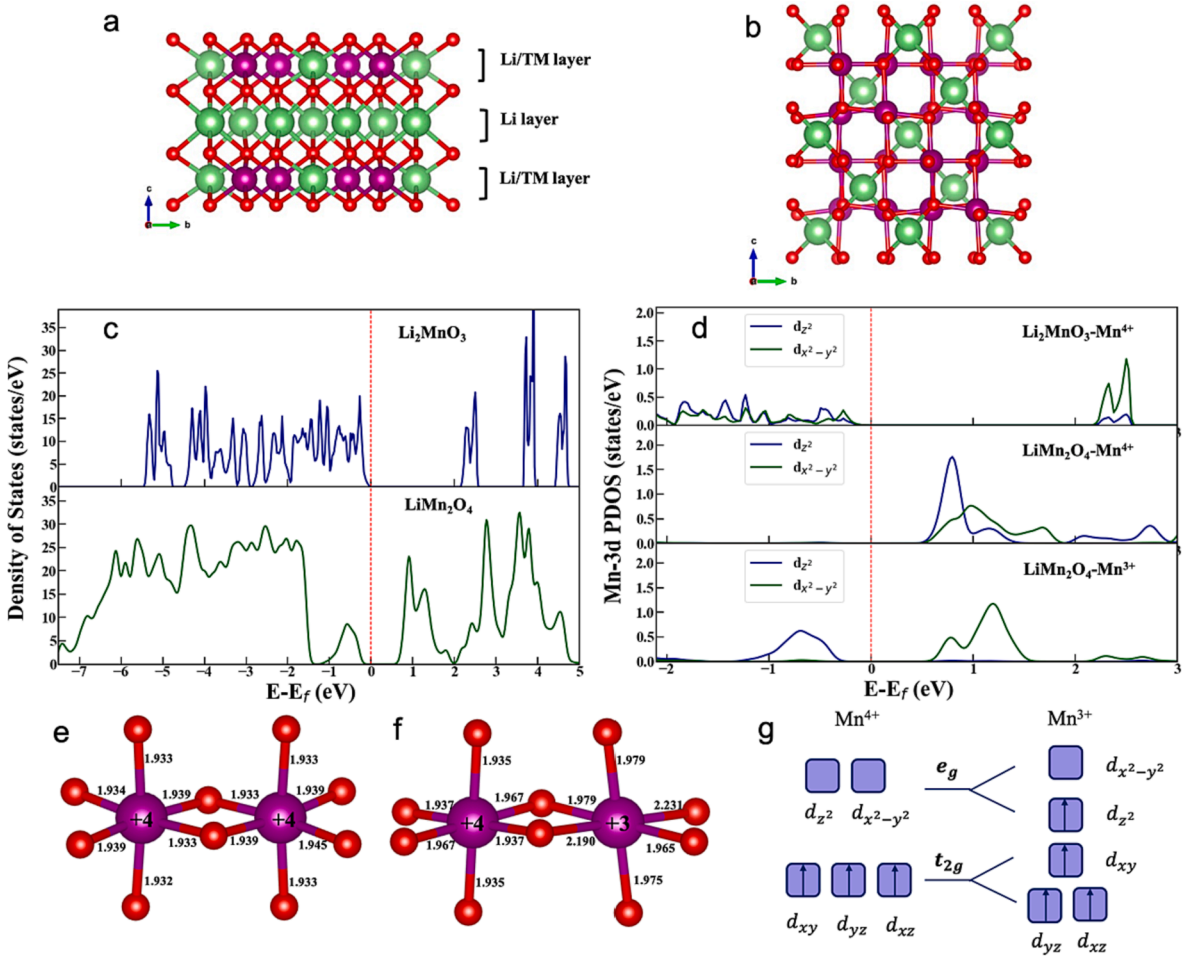

Fig. 1. The crystal structure and density of states (DOS) of layered Li_2MnO_3 and spinel $LiMn_2O_4$. a, b) The conventional cell of Li_2MnO_3 and $LiMn_2O_4$. **c)** The total DOS of Li_2MnO_3 and $LiMn_2O_4$. **d)** The Mn-3d PDOS. The Fermi levels set to be 0 eV. **e, f)** Local atomic positions around Mn atoms in the optimized Li_2MnO_3 and $LiMn_2O_4$ structures, respectively. Notations "+3" and "+4" on each Mn atom indicate the corresponding valence states. **g)** The triplet and the duplet of the d-orbit are split to e_g and t_{2g}, respectively. The two orbitals of the e_g are labeled as $d_{x^2-y^2}$ and d_{z^2}, respectively. The three orbitals of the t_{2g} are labeled as d_{xy}, d_{xz}, and d_{yz}, respectively. The green, purple and red spheres represent Li, Mn and O atoms, respectively.

3. Results

• The crystal and electronic structures

The conventional unit cells for layered Li_2MnO_3 and the spinel $LiMn_2O_4$ are illustrated in Fig. 1 (a) and (b). For the Li_2MnO_3, both antiferromagnetic (AFM) spin configuration and ferromagnetic (FM) spin configuration have been reported experimentally.[25] The calculated total energies of Li_2MnO_3 with the FM and AFM spin configuration are −37.109 and −37.097 eV per formula, respectively, indicating there is little difference in the stability of these two configurations. Unlike Li_2MnO_3, only the AFM cubic configuration for the spinel $LiMn_2O_4$ can been observed experimentally at room temperature, due to the completely disordered Mn^{3+}/Mn^{4+} arrangement, which will transform to orthorhomic structure with the descrease of temperature.[25,26] Ou *et al.* found that $LiMn_2O_4$ with the AFM orthorhombic configuration has the lower total energy at 0 K compared with the constrained cubic cell based on DFT calculation, while the predicted properties of latter are not in consistency with experiment.[27] Considering the feasible cell size to be simulated for disordered Mn^{3+}/Mn^{4+} distribution, the geometry parameters, electronic structure, and phonon band structure calculations of $LiMn_2O_4$ presented in this paper are obtained from the AFM orthorhombic structure.[27,28] The AIMD results of $LiMn_2O_4$ for the higher temperatures were obtained based on the cubic structure model regardless of the magnetic orderings. The optimized lattice parameters of Li_2MnO_3 and $LiMn_2O_4$ as well as the experimental values are listed in Table. 1. The optimized lattice parameters of Li_2MnO_3 FM and AFM structure are similar and the space group is C2/m. Li atoms are quadridentate (LiO_4) in $LiMn_2O_4$ and *hexa*-coordinate (LiO_6) in Li_2MnO_3, as shown in Fig. 1(a, b). The Mn atoms in two materials both occupy the octahedral positions forming MnO_6. There are 75% Li vacancies in $LiMn_2O_4$ and none in Li_2MnO_3.

The density of states (DOS) of Li_2MnO_3 and $LiMn_2O_4$ in Fig. 1 (c) indicate that both of them are semiconductors, but the bandgap of Li_2MnO_3 (2.1 eV) is much larger than that of $LiMn_2O_4$ (0.36 eV), which is in agreement with the experimental and other calculated results.[29,30] The difference of DOS between Mn^{3+} and Mn^{4+} leads to the different bandgap between Li_2MnO_3 and $LiMn_2O_4$ was shown in Fig. 1 (c). and the PDOS of Li, Mn, O in Li_2MnO_3 and $LiMn_2O_4$ were shown in Figure S1. Due to the Jahn-Teller effect for Mn^{3+} in $LiMn_2O_4$, the d_{z^2} of Mn^{3+} will split from $d_{x^2-y^2}$ and locate below the fermi energy and reduce the band gap, which is different from the degenerate d_{z^2} and $d_{x^2-y^2}$ for Mn^{4+} in Li_2MnO_3 as well as in $LiMn_2O_4$. The charges transfer from Mn^{3+} to O and enhance the stability of oxygen.[31] This phenomenon promotes Li-ion diffusion between the Li and transition metal layers. The projected density of states (PDOS) and corresponding electronic configuration of the Mn^{3+} ion and Mn^{4+} ion in the Li_2MnO_3 and $LiMn_2O_4$ are shown in Fig. 1 (d). The d_{z^2} orbital of the Mn^{3+} ion is below the Fermi level, while the d_{z^2} orbital of the Mn^{4+} is above the Fermi level.[32] This split effect of e_g lowers the electrostatic repulsion between the electrons of center Mn^{3+} atom and electrons in d_{z^2} orbital, and thus lowering the energy of the system.[27].

According to Fig. 1(e) and (f), it can be seen that the six bond lengths of Mn-O in Li_2MnO_3 range from 1.932 to 1.939 Å, while the bond lengths of Mn-O in $LiMn_2O_4$ range from 1.935 to 2.231 Å with four short and two long Mn–O bonds because of the Jahn-Teller effect for Mn^{3+}.[36] Thus, there are two kinds of MnO_6 in $LiMn_2O_4$ and one in Li_2MnO_3. To compare the local environments of Mn atoms in the two compounds in more detail, we employed the continuous symmetry measures (CSM) [37,38] to describe the distortion of MnO_6. The CSMs of MnO_6 for Mn^{3+} in $LiMn_2O_4$ are larger than those in Li_2MnO_3 as shown in the Table. 1, because the Mn^{3+} in $LiMn_2O_4$ partially occupies t_{2g} and e_g orbitals and leads to the Jahn-Teller effect with the t_{2g} orbital split into d_{xy}, d_{yz}, and d_{xz}, and the e_g split into $d_{x^2-y^2}$ and d_{z^2}, as shown in Fig. 1(g).[27,39] Because the Jahn-Teller effect reduces the symmetry and the degeneracy of the orbital for Mn-O, it reduces the energy of the system and stabilizes the structure. The CSMs of MnO_6 for Mn^{3+} is 1.454 in $LiMn_2O_4$, larger than 0.351 in Li_2MnO_3 as shown in the Table. 1. The migration barrier of Li_2MnO_3 is 0.762 eV, larger than that in $LiMn_2O_4$, 0.478 eV. Thus, the larger CSM in $LiMn_2O_4$ seems to help Li ion transport and enhance the Li ionic conductivity.

• Phonon density of states

Fig. 2 (a) shows the phonon density of states of Li, Mn, and O atoms for Li_2MnO_3 and $LiMn_2O_4$ based on the harmonic oscillation approximation. The results show that there is no imaginary frequency, indicating that both phases are dynamically stable. Moreover, the medium-to-low frequency modes mainly correspond to Li atoms and transition metal atoms, while the high-frequency modes above 14 THz are mainly associated with the vibration of O atoms and transition metal atoms.[40] Yang *et al* reported that the phonon band center presents the softness of lattice dynamics.[41] They proposed that the calculated Li phonon band center is correlated with the ionic conductivity. And the lower phonon frequencies showed the lower activation energy. The phonon band center ω_{av} (the average frequency), the centroid of the phonon density of states, evaluates the average vibrational frequency of the material, which can be expressed by the following equation.[38]

$$\omega_{av} = \frac{\int \omega PDOS(\omega)}{\int PDOS(\omega) d\omega} \tag{1}$$

where the $PDOS(\omega)$ is the atom-projected phonon DOS and ω_{av} represents the phonon band center.

As shown in Fig. 2, the band centers of PDOS for Li in Li_2MnO_3 with the AFM configuration and the FM configuration are 10.81 THz and 10.82 THz, respectively, which are lower compared with the $LiMn_2O_4$ (11.54 THz). Similar to our study, an increased activation energy was observed in $Li_{10}Ge_{1-x}Sn_xP_2S$ with softer lattice,[42] which was believed to be related to the stronger local ionic bonding interactions between Li^+ and S^{2-}. The bond lengths of Mn-O in Li_2MnO_3 range from 1.932 to 1.939 Å, which is smaller than the bond lengths of Mn-O in $LiMn_2O_4$ ranging from 1.935 to 2.231 Å. Thus, the average bader charge of O in Li_2MnO_3 (-1.21e) is more negative than that in $LiMn_2O_4$ (-1.13e),

Table 1
Optimized Lattice Parameters of Li_2MnO_3 and $LiMn_2O_4$ (/Å) .

	a	b	c	α	β	γ	Method	CSM of MnO_6	space group	Magnetic
Li_2MnO_3	5.01	8.66	5.09	90.0	109.4	90.0	This work	0.347	C2/m	FM
	5.00	8.65	5.10	90.0	109.4	90.0	This work	0.351	C2/m	AFM
	4.98	8.62	5.07	90.0	109.4	90.0	DFT[33]	–	C2/m	–
	4.94	8.53	5.02	90.0	109.3	90.0	Exp.[34]	–	C2/m	–
$LiMn_2O_4$	8.22	8.22	8.75	90.0	90.0	89.6	This work	1.454 0.304	P1	AFM
	8.17	8.17	8.17	90.0	90.0	90.0	This work	–	Fd $\bar{3}$ m	FM
	8.20	8.20	8.74	90.0	90.0	90.0	DFT[10]	–	Fd $\bar{3}$ m	AFM
	8.29	8.29	8.29	90.0	90.0	90.0	DFT[35]	–	Fd $\bar{3}$ m	FM
	8.24	8.24	8.24	90.0	90.0	90.0	Exp.[34]	–	Fd $\bar{3}$ m	AFM

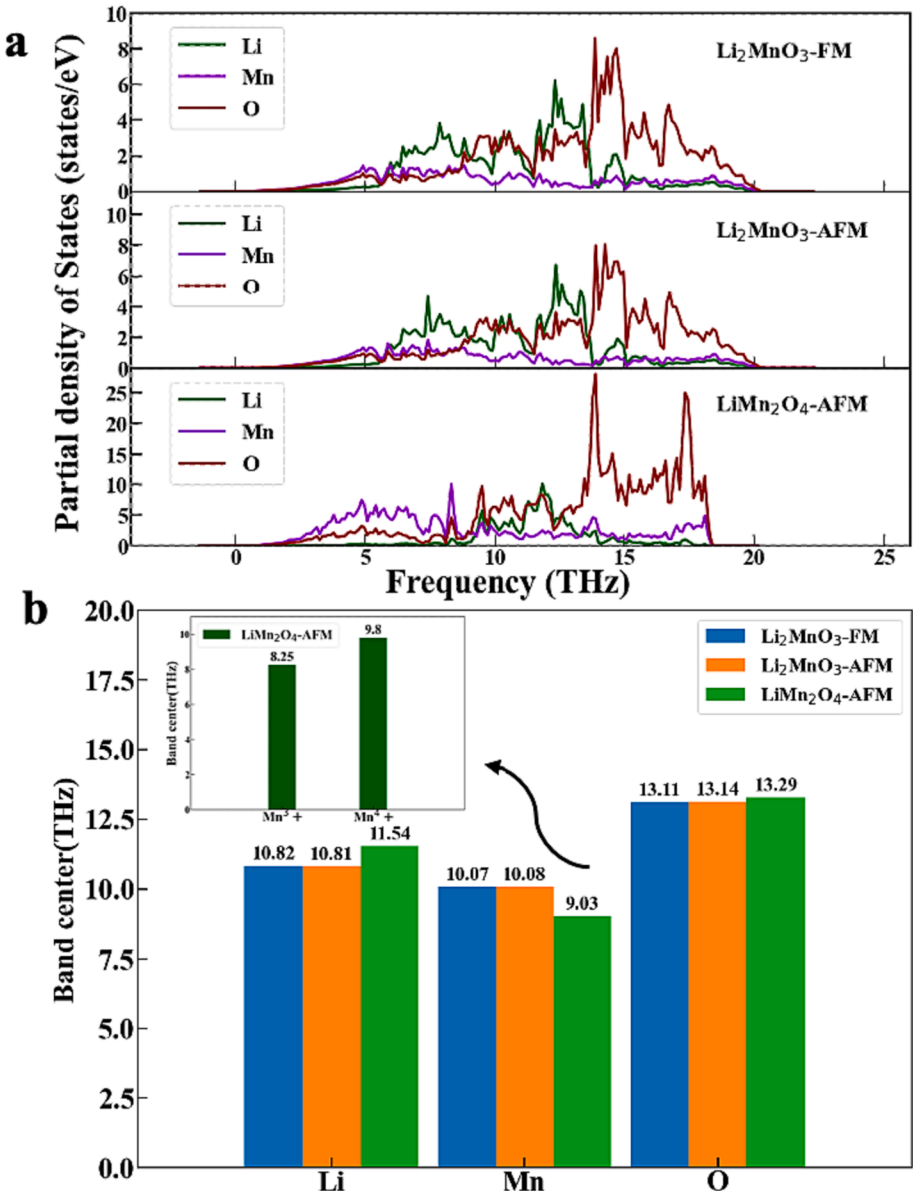

Fig. 2. The phonon density of states for Li_2MnO_3 and $LiMn_2O_4$. a) The partial phonon density of states of layered Li_2MnO_3 and spinel $LiMn_2O_4$. b) The band center of Li, Mn and O partial phonon density of states.

leading to a larger Coulombic interaction between Li and O and hence a higher Li migration barrier in layered Li_2MnO_3 with soft lattice. However, the difference (2.29 THz or 2.23 THz) between the band center of Li and O in Li_2MnO_3 is larger compared with that in the $LiMn_2O_4$ (1.74 THz). The band center of PDOS for Mn (10.07 THz or 10.08 THz) in Li_2MnO_3 is higher compared with $LiMn_2O_4$ (9.03 THz). The Mn^{3+} and Mn^{4+} ions in $LiMn_2O_4$ make the interaction of the partially elongated Mn-O atoms weak due to the Jahn-Teller distortion resulting in the lower vibration frequency of Mn.[43] The Mn^{3+} partial density of states appear in the lower frequency with the band center of Mn^{3+} to be 8.25 THz, as shown in Fig. 2 (b). The band centers of PDOS for O atoms in the two cathode materials are similar.

- **Diffusion and energy barriers**

Fig. 3 (a) shows that the conductivity of Li ions increases gradually for $LiMn_2O_4$ and Li_2MnO_3 as the temperature increases. In addition, it is found that the calculated conductivity of Li ions in $LiMn_2O_4$ is much higher compared with Li_2MnO_3. The energy barriers of Li ions diffusions determined from the AIMD and the NEB calculation are listed in Table 2. The migration energy barriers of Li ions in Li_2MnO_3 by the AIMD and the NEB calculation are 0.762 eV and 0.558 eV, respectively, which are in excellent agreement with the previously calculation value of 0.610 eV.[29] It's worth noting that the migration energy barriers of Li ions by different calculation methods in $LiMn_2O_4$, 0.478 eV and 0.347 eV obtained from AIMD and NEB simulations, respectively, are lower compared with those in Li_2MnO_3, which indicates that Li ions migrate more easily in $LiMn_2O_4$ than in Li_2MnO_3.

The Li of $LiMn_2O_4$ migrates between two adjacent tetrahedrons through an octahedron. The path of Li migration of Li_2MnO_3 are two adjacent octahedrons through the middle tetrahedron vacancy. In general, results show that Li has a better migration ability in $LiMn_2O_4$ than Li_2MnO_3 because of layered Li_2MnO_3 with all Li sites being occupied and spinel $LiMn_2O_4$ with Li vacancies. The $LiMn_2O_4$ has a fast migration channel compared with Li_2MnO_3.

Based on the ionic trajectories from AIMD simulations at 1000 K, 1100 K, 1300 K, 1500 K, and 2100 K, we also calculated the van hove correlation function to compare the migration behaviors of Li ions in the

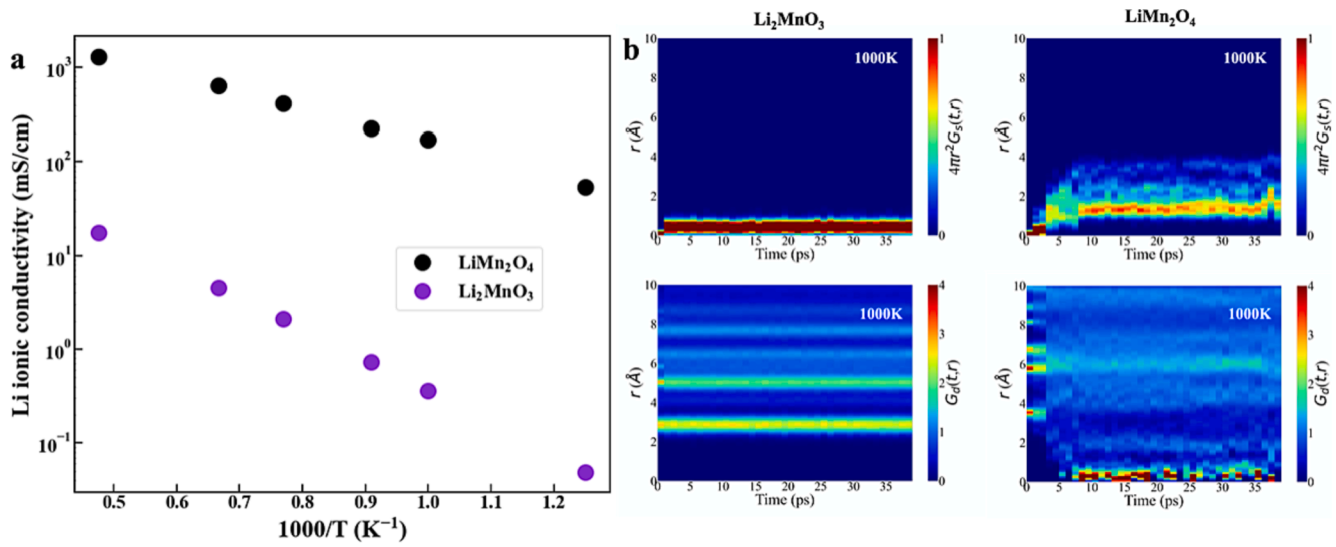

Fig. 3. The Li ionic conductiviuty and the van Hove correlation function for Li_2MnO_3 and $LiMn_2O_4$ at different temperatures. a) The Li ionic conductivities of Li_2MnO_3 and $LiMn_2O_4$; **b)** Plots of the self (G_s) and distinct-part of the van Hove correlation function (G_d) for Li_2MnO_3 and $LiMn_2O_4$ at 1000 K. G_s is a function of the Li distance r and time t. G_d is a function of the Li-Li pair distance r and time t.

Table 2
Migration barriers of Li_2MnO_3 and $LiMn_2O_4$.

Structure	Migration barriers/eV	Source
Li_2MnO_3	0.558	NEB-Cal. this work
	0.762	AIMD-Cal. this work
	0.610	NEB-Cal[29]
$LiMn_2O_4$	0.347	NEB-Cal. this work
	0.478	AIMD-Cal. this work
	0.560	Procrystal analysis-Cal[44]
	0.350	NEB-Cal[35]
	0.33 ~ 0.375	Exp[45,46]

Li_2MnO_3 and $LiMn_2O_4$ cathode materials. Fig. 3 (b) presents the self of the van Hove correlation function G_s and the distinct part of the van Hove correlation function G_d for Li_2MnO_3 and $LiMn_2O_4$ at 1000 K. The results of G_s show that Li in Li_2MnO_3 is almost immovable but Li diffuses faster in $LiMn_2O_4$. The results show that there is a peak found in the $LiMn_2O_4$ structure at the proximity of r = 0 according to the G_d, indicating there is a synergistic effect between the Li ions in $LiMn_2O_4$, but the similar effect does not exist in Li_2MnO_3. Figure S2 presents the Li ion motions in $LiMn_2O_4$ are highly correlated at all temperatures considered and enhanced with temperatures. This observation is consistent with the result of the higher diffusion coefficient found in the spinel $LiMn_2O_4$ structure.

- **Doping with transition metals (TM)**

It has been reported that the doping of transition metals Ir, Os and Ru on the surface of layered Li_2MnO_3 can improve its stability due to the decreased O loss and thus prevent the phase transition into the spinel-type. Therefore, taking Ir, Os and Ru with the valence state of + 4 as examples, we investigated the effects of element doping on the migration ability of Li ions in Li_2MnO_3. A transition metal atom is used to replace the Mn atom, and the structure of Li_2MnO_3 after doping is shown in Fig. 4 (a). The migration energy barriers of Li ions in the pristine Li_2MnO_3 and the doped Li_2MnO_3 are presented in Fig. 4 (b) by the BVPA method. It can be found from Fig. 4 (b) that the migration energy barriers of Li ions in the Li_2MnO_3 after doping are lower compared with the pristine Li_2MnO_3. The radius of Os(1.85 Å) is large than Ir(1.80 Å) and Ru(1.78 Å), inducing larger structural distortion. So, the Li migration energy barrier of Li_2MnO_3 upon Os doping is smaller than Ir and Ru doping. Therefore, doping Mn in Li_2MnO_3 is an effective method to increase the migration ability of Li ions. Combined with the experimental

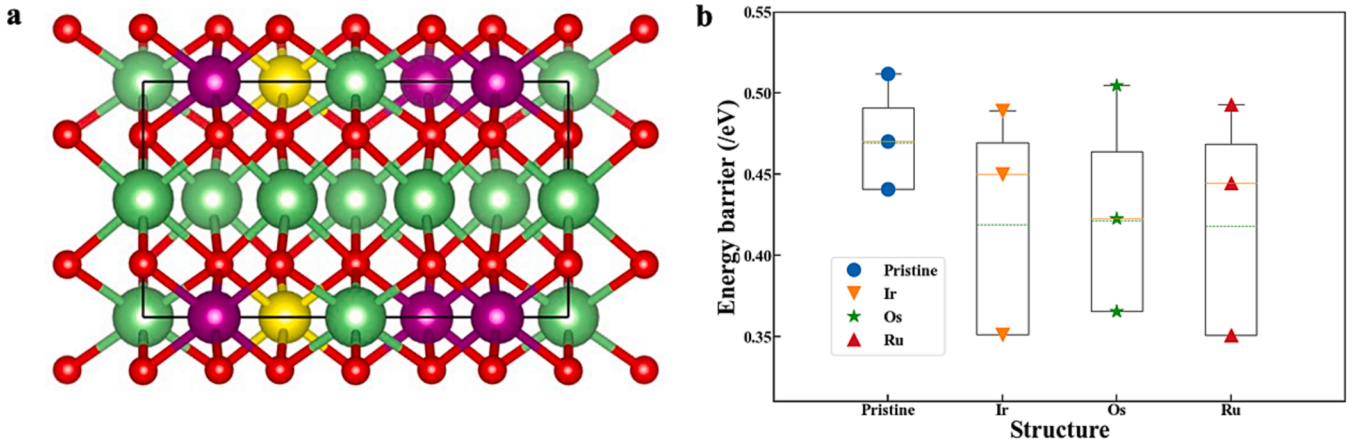

Fig. 4. The migration energy barrier of Li in Li_2MnO_3 doped with transition metals (TM = Ir, Os, Ru) The green, purple, yellow, and red spheres represent Li, Mn, TM, and O atoms, respectively.

results that doping can improve the surface stability,[8,47,48] the increase of Li migration ability can improve the overall stability of Li_2MnO_3 from the lithium dynamics and thermal stability points of view.

4. Conclusions

In this work, the electronic structure, phonon spectrum and Li diffusion of Li_2MnO_3 and $LiMn_2O_4$ are studied through DFT calculations combined with phonopy. The bandgap of Li_2MnO_3 is larger than $LiMn_2O_4$. The anti-ferromagnetic (AFM) configurations of Li_2MnO_3 and $LiMn_2O_4$ are stable through the phonon spectrum. The electronic structures and stability of Li_2MnO_3 and $LiMn_2O_4$ are similar. $LiMn_2O_4$ is not fully occupied structure and has synergies with fast-ion channels compared with Li_2MnO_3. The migration effect of Li-ion is improved by doping in Li_2MnO_3. Our results show the reason that the stability of Li_2MnO_3 can be improved by doping, because doping with Ir, Os and Ru elements reducing the Li migration barrier reduces the Li migration barrier as low as that in $LiMn_2O_4$. This work indicates the importance to enhance the stability of the Li_2MnO_3 cathode electrode through faster Li transport.

CRediT authorship contribution statement

Jialiang Xu: Conceptualization, Methodology, Formal analysis, Data curation, Writing – original draft, Validation, Writing – review & editing. **Shiji Zhu:** Data curation, Visualization, Investigation. **Zhenming Xu:** Formal analysis, Writing – review & editing. **Hong Zhu:** Supervision.

Declaration of Competing Interest

The authors declare that they have no known competing financial interests or personal relationships that could have appeared to influence the work reported in this paper.

Data availability

Data will be made available on request.

Acknowledgments

This work was supported by the National Natural Science Foundation of China (52072240) and the Materials Genome Initiative Center at Shanghai Jiao Tong University. All simulations were performed at the Shanghai Jiao Tong University High Performance Computing Center.

Appendix A. Supplementary data

Supplementary data to this article can be found online at https://doi.org/10.1016/j.commatsci.2023.112426.

References

[1] B.C. Melot, J.-M. Taroscon, Design and Preparation of Materials for Advanced Electrochemical Storage, Acc Chem Res. 46 (5) (2013) 1226–1238, https://doi.org/10.1021/ar300088q.
[2] J. Marzec, Conduction mechanism in operating a LiMn2O4 cathode, Solid State Ion. 146 (3–4) (2002) 225–237, https://doi.org/10.1016/S0167-2738(01)01022-0.
[3] A. Van der Ven, M.K. Aydinol, G. Ceder, G. Kresse, J. Hafner, First-principles investigation of phase stability in Li x CoO 2, Phys. Rev. B 58 (6) (1998) 2975–2987, https://doi.org/10.1103/PhysRevB.58.2975.
[4] P. Yan, L. Xiao, J. Zheng, Y. Zhou, Y. He, X. Zu, S.X. Mao, J. Xiao, F. Gao, J.-G. Zhang, C.-M. Wang, Probing the degradation mechanism of Li $_2$ MnO $_3$ cathode for Li-Ion batteries, Chem. Mater. 27 (3) (2015) 975–982, https://doi.org/10.1021/cm504257m.
[5] J. Rana, M. Stan, R. Kloepsch, J. Li, G. Schumacher, E. Welter, I. Zizak, J. Banhart, M. Winter, Structural changes in Li $_2$ MnO $_3$ cathode material for Li-Ion batteries, Adv. Energy Mater. 4 (5) (2014) 1300998, https://doi.org/10.1002/aenm.201300998.
[6] B. Xu, C.R. Fell, M. Chi, Y.S. Meng, Identifying surface structural changes in layered li-excess nickel manganese oxides in high voltage lithium ion batteries: A joint experimental and theoretical study, Energy Environ. Sci. 4 (6) (2011) 2223, https://doi.org/10.1039/c1ee01131f.
[7] F. Lin, I.M. Markus, D. Nordlund, T.-C. Weng, M.D. Asta, H.L. Xin, M.M. Doeff, Surface reconstruction and chemical evolution of stoichiometric layered cathode materials for lithium-ion batteries, Nat. Commun. 5 (1) (2014) 3529, https://doi.org/10.1038/ncomms4529.
[8] Y. Shin, W.H. Kan, M. Aykol, J.K. Papp, B.D. McCloskey, G. Chen, K.A. Persson, Alleviating oxygen evolution from Li-Excess oxide materials through theory-guided surface protection, Nat. Commun. 9 (1) (2018) 4597, https://doi.org/10.1038/s41467-018-07080-6.
[9] J. Peng, Y. Li, Z. Chen, G. Liang, S. Hu, T. Zhou, F. Zheng, Q. Pan, H. Wang, Q. Li, J. Liu, Z. Guo, Phase compatible NiFe $_2$ O 4 coating tunes oxygen redox in Li-Rich layered oxide, ACS Nano 15 (7) (2021) 11607–11618, https://doi.org/10.1021/acsnano.1c02023.
[10] X. Li, J. Wang, S. Zhang, L. Sun, W. Zhang, F. Dang, H.J. Seifert, Y. Du, Intrinsic defects in LiMn $_2$ O 4: First-principles calculations, ACS Omega 6 (33) (2021) 21255–21264, https://doi.org/10.1021/acsomega.1c01162.
[11] M.L. de Victoria, L. Torres-Castro, R.K. Katiyar, J. Shojan, V. Dorvilien, R.S. Katiyar Synthesis, Characterization, and electrochemical analysis of the cobalt free composite cathode material 0.5Li2MnO3-0.25LiMn2O4-0.25LiNi0.5Mn0.5O2 for lithium ion batteries applications, MRS Adv. 1 (45) (2016) 3063–3068, https://doi.org/10.1557/adv.2016.515.
[12] D.S. Sholl, J.A. Steckel, Density functional theory: A practical introduction, John Wiley & Sons, 2011.
[13] J. Hafner, *Ab-Initio* simulations of materials using VASP: Density-functional theory and beyond, J. Comput. Chem. 29 (13) (2008) 2044–2078, https://doi.org/10.1002/jcc.21057.
[14] G. Kresse, J. Furthmüller, Efficient iterative schemes for *Ab Initio* total-energy calculations using a plane-wave basis set, Phys. Rev. B 54 (16) (1996) 11169–11186, https://doi.org/10.1103/PhysRevB.54.11169.
[15] P.E. Blöchl, O. Jepsen, O.K. Andersen, Improved tetrahedron method for brillouin-zone integrations, Phys. Rev. B 49 (23) (1994) 16223–16233, https://doi.org/10.1103/PhysRevB.49.16223.
[16] W. Kohn, L.J. Sham, Self-consistent equations including exchange and correlation effects, Phys. Rev. 140 (4A) (1965) A1133–A1138, https://doi.org/10.1103/PhysRev.140.A1133.
[17] S.L. Dudarev, G.A. Botton, S.Y. Savrasov, C.J. Humphreys, A.P. Sutton, Electron-energy-loss spectra and the structural stability of nickel oxide: An LSDA+U study, Phys. Rev. B 57 (3) (1998) 1505–1509, https://doi.org/10.1103/PhysRevB.57.1505.
[18] J.P. Perdew, K. Burke, M. Ernzerhof, Generalized gradient approximation made simple [Phys. Rev. Lett. 77, 3865 (1996)], *Phys. Rev. Lett.* 78 (7) (1997) 1396, https://doi.org/10.1103/PhysRevLett.78.1396.
[19] M.D. Radin, J. Vinckeviciute, R. Seshadri, A. Van der Ven, Manganese oxidation as the origin of the anomalous capacity of Mn-containing Li-excess cathode materials, Nat. Energy 4 (8) (2019) 639–646, https://doi.org/10.1038/s41560-019-0439-6.
[20] F. Zhou, M. Cococcioni, C.A. Marianetti, D. Morgan, G. Ceder, First-principles prediction of redox potentials in transition-metal compounds with LDA + U, Phys. Rev. B 70 (23) (2004), 235121, https://doi.org/10.1103/PhysRevB.70.235121.
[21] Y. Koyama, I. Tanaka, M. Nagao, R. Kanno, First-principles study on lithium removal from Li2MnO3, J. Power Sources 189 (1) (2009) 798–801, https://doi.org/10.1016/j.jpowsour.2008.07.073.
[22] A. Togo, I. Tanaka, First principles phonon calculations in materials science, *ArXiv150608498 Cond-Mat* (2015).
[23] G. Henkelman, H. Jónsson, Improved tangent estimate in the nudged elastic band method for finding minimum energy paths and saddle points, J. Chem. Phys. 113 (22) (2000) 9978–9985, https://doi.org/10.1063/1.1323224.
[24] L.L. Wong, K.C. Phuah, R. Dai, H. Chen, W.S. Chew, S. Adams, Bond valence pathway analyzer—an automatic rapid screening tool for fast ion conductors within softBV, Chem. Mater. 33 (2) (2021) 625–641, https://doi.org/10.1021/acs.chemmater.0c03893.
[25] X. Zhang, S. Tang, Y. Du, Synthesis and magnetic properties of antiferromagnetic Li2MnO3 nanoribbons, Phys. Lett. A 375 (36) (2011) 3196–3199, https://doi.org/10.1016/j.physleta.2011.07.008.
[26] K. Hoang, Understanding the electronic and ionic conduction and lithium over-stoichiometry in LiMn $_2$ O 4 spinel, J Mater Chem A 2 (43) (2014) 18271–18280, https://doi.org/10.1039/C4TA04116J.
[27] C.Y. Ouyang, S.Q. Shi, M.S. Lei, Jahn-teller distortion and electronic structure of LiMn2O4, J. Alloys Compd. 474 (1–2) (2009) 370–374, https://doi.org/10.1016/j.jallcom.2008.06.123.
[28] W.-W. Liu, D. Wang, Z. Wang, J. Deng, W.-M. Lau, Y. Zhang, Influence of magnetic ordering and jahn-teller distortion on the lithiation process of LiMn $_2$ O 4, Phys. Chem. Chem. Phys. 19 (9) (2017) 6481–6486, https://doi.org/10.1039/C6CP08324B.
[29] R. Xiao, H. Li, L. Chen, Density functional investigation on Li $_2$ MnO $_3$, Chem. Mater. 24 (21) (2012) 4242–4251, https://doi.org/10.1021/cm3027219.
[30] Z.Q. Wang, Y.C. Chen, C.Y. Ouyang, Polaron states and migration in F-Doped Li2MnO3, Phys. Lett. A 378 (32–33) (2014) 2449–2452, https://doi.org/10.1016/j.physleta.2014.06.025.
[31] Y. Gao, J. Ma, X. Wang, X. Lu, Y. Bai, Z. Wang, L. Chen, Improved electron/li-ion transport and oxygen stability of mo-doped Li2MnO3, J. Mater. Chem. A 2 (13) (2014) 4811, https://doi.org/10.1039/c3ta15236g.

[32] W. Hu, W.-W. Luo, M.-S. Wu, B. Xu, C.-Y. Ouyang, Configurational entropy-induced phase transition in spinel LiMn $_{2}$ $_{O}$ 4, Chin. Phys. B 31 (9) (2022), 098202, https://doi.org/10.1088/1674-1056/ac6863.
[33] Li, Q. Improving the Oxygen Redox Reversibility of Li-Rich Battery Cathode Materials via Coulombic Repulsive Interactions Strategy. 13.
[34] B. Li, Z. Dang, Y. Zhang, Z. Song, Synthesis and lithium storage properties of Li-Mn-O compounds: Crystal growth of LiMn2O4 and Li2MnO3, Int J Electrochem Sci 9 (2014) 8.
[35] M. Nakayama, M. Kaneko, M. Wakihara, First-principles study of lithium ion migration in lithium transition metal oxides with spinel structure, Phys. Chem. Chem. Phys. 14 (40) (2012) 13963, https://doi.org/10.1039/c2cp42154b.
[36] R. Arabolla Rodríguez, M. González Montiel, N. Della Santina Mohallem, Y. Mosqueda Laffita, L. Andrey Montoro, M. Avila Santos, H. León Ramírez, E. L. Pérez-Cappe, The role of defects on the jahn-teller effect and electrochemical charge storage in nanometric LiMn2O4 material, Solid State Ion. 369 (2021), https://doi.org/10.1016/j.ssi.2021.115707.
[37] M. Pinsky, D. Avnir, Continuous symmetry measures. 5. The classical polyhedra, Inorg. Chem. 37 (21) (1998) 5575–5582, https://doi.org/10.1021/ic9804925.
[38] D. Waroquiers, X. Gonze, G.-M. Rignanese, C. Welker-Nieuwoudt, F. Rosowski, M. Göbel, S. Schenk, P. Degelmann, R. André, R. Glaum, G. Hautier, Statistical analysis of coordination environments in oxides, Chem. Mater. 29 (19) (2017) 8346–8360, https://doi.org/10.1021/acs.chemmater.7b02766.
[39] Y. Ma, L. lv, Y. Dai, Q. Zhou, J. Cheng, H. Li, W. Hu, A first-principles study on the structure and electronic structure of Ti-doped spinel LiMn2O4 for Li-Ion batteries, *J. Electron. Mater.* 51 (1) (2022) 77–83, https://doi.org/10.1007/s11664-021-09293-w.
[40] R. Pulido, N. Naveas, R.J. Martin-Palma, F. Agulló-Rueda, V.R. Ferró, J. Hernández-Montelongo, G. Recio-Sánchez, I. Brito, M. Manso-Silván, Phonon structure, infra-red and raman spectra of Li2MnO3 by first-principles calculations, Materials 15 (18) (2022) 6237, https://doi.org/10.3390/ma15186237.
[41] S. Muy, J.C. Bachman, L. Giordano, H.-H. Chang, D.L. Abernathy, D. Bansal, O. Delaire, S. Hori, R. Kanno, F. Maglia, S. Lupart, P. Lamp, Y. Shao-Horn, Tuning mobility and stability of lithium ion conductors based on lattice dynamics, Energy Environ. Sci. 11 (4) (2018) 850–859, https://doi.org/10.1039/C7EE03364H.
[42] T. Krauskopf, S.P. Culver, W.G. Zeier, Bottleneck of diffusion and inductive effects in Li 10 Ge 1–x Sn x P 2 S 12, Chem. Mater. 30 (5) (2018) 1791–1798, https://doi.org/10.1021/acs.chemmater.8b00266.
[43] H. Yang, C.N. Savory, B.J. Morgan, D.O. Scanlon, J.M. Skelton, A. Walsh, Chemical trends in the lattice thermal conductivity of Li(Ni, Mn, Co)O $_{2}$ (NMC) battery cathodes, Chem. Mater. 32 (17) (2020) 7542–7550, https://doi.org/10.1021/acs.chemmater.0c02908.
[44] M.Ø. Filsø, M.J. Turner, G.V. Gibbs, S. Adams, M.A. Spackman, B.B. Iversen, Visualizing lithium-ion migration pathways in battery materials, Chem. - Eur. J. 19 (46) (2013) 15535–15544, https://doi.org/10.1002/chem.201301504.
[45] Y.G. Mateyshina, U. Lafont, N.F. Uvarov, E.M. Kelder, Physical and electrochemical properties of iron-doped lithium–manganese-spinels prepared by different methods, Solid State Ion. 179 (1–6) (2008) 192–196, https://doi.org/10.1016/j.ssi.2007.12.067.
[46] D. Capsoni, M. Bini, G. Chiodelli, V. Massarotti, M.C. Mozzati, C.B. Azzoni, Structural transition in Mg-Doped LiMn2O4: A comparison with other M-Doped Li–Mn spinels, Solid State Commun. 125 (3–4) (2003) 179–183, https://doi.org/10.1016/S0038-1098(02)00769-X.
[47] Y. Sun, L. Zan, Y. Zhang, Enhanced electrochemical performances of Li2MnO3 cathode materials via adjusting oxygen vacancies content for lithium-ion batteries, Appl. Surf. Sci. 483 (2019) 270–277, https://doi.org/10.1016/j.apsusc.2019.03.210.
[48] N. Kuganathan, E. Sgourou, Y. Panayiotatos, A. Chroneos, Defect process, dopant behaviour and li ion mobility in the Li2MnO3 cathode material, Energies 12 (7) (2019) 1329, https://doi.org/10.3390/en12071329.